Journal of Hydrology 410 (2011) 248–259

Contents lists available at SciVerse ScienceDirect

Journal of Hydrology

journal homepage: www.elsevier.com/locate/jhydrol

Using ensemble of climate models to evaluate future water and solutes budgets in Lake Kinneret, Israel

Alon Rimmer [a,*], Amir Givati [b], Rana Samuels [c], Pinhas Alpert [c]

[a] Israel Oceanographic and Limnological Research Ltd., The Lake Kinneret Limnological Laboratory, Israel
[b] Israeli Hydrological Service, Water Authority, Israel
[c] Department of Geophysics and Planetary Sciences, Faculty of Exact Sciences, Tel Aviv University, Tel Aviv, Israel

ARTICLE INFO

Article history:
Received 7 March 2011
Received in revised form 14 September 2011
Accepted 18 September 2011
Available online 28 September 2011
This manuscript was handled by Konstantine P. Georgakakos, Editor-in-Chief, with the assistance of Günter Blöschl, Associate Editor

Keywords:
Climate models
Ensemble
Lake evaporation model
Lake salinity model
Available water
Lake Kinneret

SUMMARY

Identifying and quantifying future climate effects on water resources has major economic and societal implications, rendering such studies extremely important for water planners. Here we integrate output from one high resolution global (Japan Meteorological Agency) and three regional (ECHAM-RegCM, Hadley-MM5, ECHAM-MM5) climate models into three hydrological tools (1. annual incoming water volumes; 2. evaporation from the lake; and 3. lake salinity) to provide first approximations of climate change impacts on water quantity and quality in Lake Kinneret (also known as Sea of Galilee), the major freshwater resource in Israel. Meteorological data extracted from the climate models were used as input data into the models. Results were calculated for the historical 1979–2009 and the future 2015–2060 periods. The modeled historical period was verified against observed data, first by each model alone, and then by the combined model structure. Predicted results varied between the climate models. The ECHAM-RegCM predicted decreased precipitation in an average rate of ~7 mm year^{-1} (−0.8% annually) while the trends of precipitation predicted by the other models were less obvious. According to the combination of ECHAM-RegCM, ECHAM-MM5 and Hadley-MM5 with the lake evaporation model, the evaporation will increase by 0.2–0.6 Mm^3 (0.10–0.25%) annually while according to the JMA no trend was found. The lake salinity is mostly impacted by changes in inflows and therefore only the ECHAM-RegCM predicted significant increase of salinity (from 280 ppm Cl today to ~450 ppm Cl in 2060), while the trends of salinity according to other models were mild.

1. Introduction

The possible expected impacts of climate change in the Eastern Mediterranean and Middle East region are worrisome indeed. The most recent IPCC global circulation models (GCMs) as well as a recently run of 20 km mesh global climate simulation agree on a drying scenario in the region by the end of the 21st century (IPCC, 2007; Kitoh et al., 2008). Future climate is expected to be characterized by possible decreasing precipitation trends, increasing temperature and potential evaporation with an increase in extreme events (Krichak et al., 2007; Kunstmann et al., 2007; Samuels et al., 2009).

A significant decrease in rainfall, spring flow and stream flow has been recently documented both in the Jordan River basin (Givati and Rosenfeld, 2007, 2011) as well as in the Litani basin in Lebanon (Shaban, 2009). Based on statistical analysis of the Arctic Oscillation (AO) vs. precipitation trends, together with physical considerations and synoptic observations, Givati and Rosenfeld (2011) imply that the observed precipitation trends in Israel can be explained by shifts in the AO driven by greenhouses global warming. They suggest that the continuation of the AO positive trend as showed in the IPCC projections will lead to decreasing trend in precipitation in Northern Israel (The Lake Kinneret basin) and so to a substantial loss of water resources that has already occurred. Decreased precipitation and increase of temperature are expected to reduce aquifer replenishment and the stream flow of rivers, and increase evaporation from open water sources, respectively. Together with the projected increases in future water demands, increased stress on water supply systems is expected, due to further deterioration of water quality in both surface and groundwater sources. A major concern in Israel is the enhanced salinization process of Lake Kinneret in the north (Rimmer, 2008). Although it is expected that desalination will play an increasingly larger role with respect to water supply, natural water sources will remain important both for consumption as well as for maintaining the natural rivers, flora and fauna of the north. Hence, availability and quality changes in the natural water will remain a

* Corresponding author. Address: Israel Oceanographic and Limnological Research Ltd., The Kinneret Limnological Laboratory, PO Box 447, Migdal 14950, Israel. Fax: +972 4 6724627.
E-mail address: alon@ocean.org.il (A. Rimmer).

0022-1694/$ - see front matter © 2011 Elsevier B.V. All rights reserved.
doi:10.1016/j.jhydrol.2011.09.025

critical issue. Efforts must be made to predict the future availability and quality of water, while protecting it and using it effectively.

Our purpose in this study is to establish water management decision support system (DSS), by connecting several types of high resolution global climate models into a cascade of hydrological models. The proposed model structure provides a platform for predicting long term (decadal) changes in two of the most significant variables of the surface water in the Lake Kinneret basin: the available water volume (AW) and its attributed salinity.

The objectives of this paper in particular are:

1. To combine climate and hydrological models to predict long term patterns of water availability and water quality (solute concentration, expressed by ppm Cl^-) in the Lake Kinneret basin.
2. To explain how these models may contribute to improve the water management of hydrological systems that are affected by climate change.
3. To provide a first ensemble of predictions for the expected changes of water availability and quality in the region.

The current study is limited to driving the hydrological models with four different climate models. These are currently the global and regional climate models available at a spatial resolution of ~20 km and hence are the best available models for the region. All models have been proven to effectively capture past trends in the region, even outperforming re-analysis data (Jin et al., 2010, 2011; Krichak et al., 2011; Smiatek et al., 2011). However, given the limitation that only four models are used, the results should be seen as a first approximation. Nevertheless, the modular form of the proposed model combination enables easy improvement and validation of the results, based on input from additional climate models as they become available.

2. Study region

The area of the Lake Kinneret watershed is 2730 km^2 (*see* Fig. 1). The 165 km^2 lake, located in the central part of the Jordan Rift Valley (Northern Israel), is the most important surface water resource in Israel, providing approximately 35% of the annual drinking water to a population of almost 7.5 million inhabitants. The major water source of the lake is the ~1600 km^2 of the Upper Catchments of the Jordan River (UCJR) where ~920 km^2 are in Israel with the remainder located in Syria and Lebanon. The high elevation of the Mount Hermon range (between 1200 and 2800 m) in the north of the UCJR is the wettest area in the Lake Kinneret watershed with average annual precipitation ranging between 1200 and 1500 mm. The Mt. Hermon basins feed the three major tributaries of the Jordan River (Rimmer and Salingar, 2006): the Dan with ~250 million m^3 (Mm^3) annually, the Hermon (~110 Mm^3, also known as Banias), and the Snir (~115 Mm^3, also known as the Hazbani River). The other part of the Lake Kinneret basin is the direct watershed, located in the immediate vicinity of the lake. The area of the direct watershed is ~965 km^2, where 577 km^2 are the southern part of the Golan Heights in the east, and the other 388 km^2 are part of the Eastern Galilee Mountains to the west of the lake.

The average annual water inflows to Lake Kinneret over the past decades are 660 Mm^3 (for the period 1979–2009) including the Jordan River (455 Mm^3), direct rainfall (65 Mm^3), direct watershed runoff and artificial diversion from the Yarmuk River (100 Mm^3), and springs (40 Mm^3) flowing directly into the lake (Israel

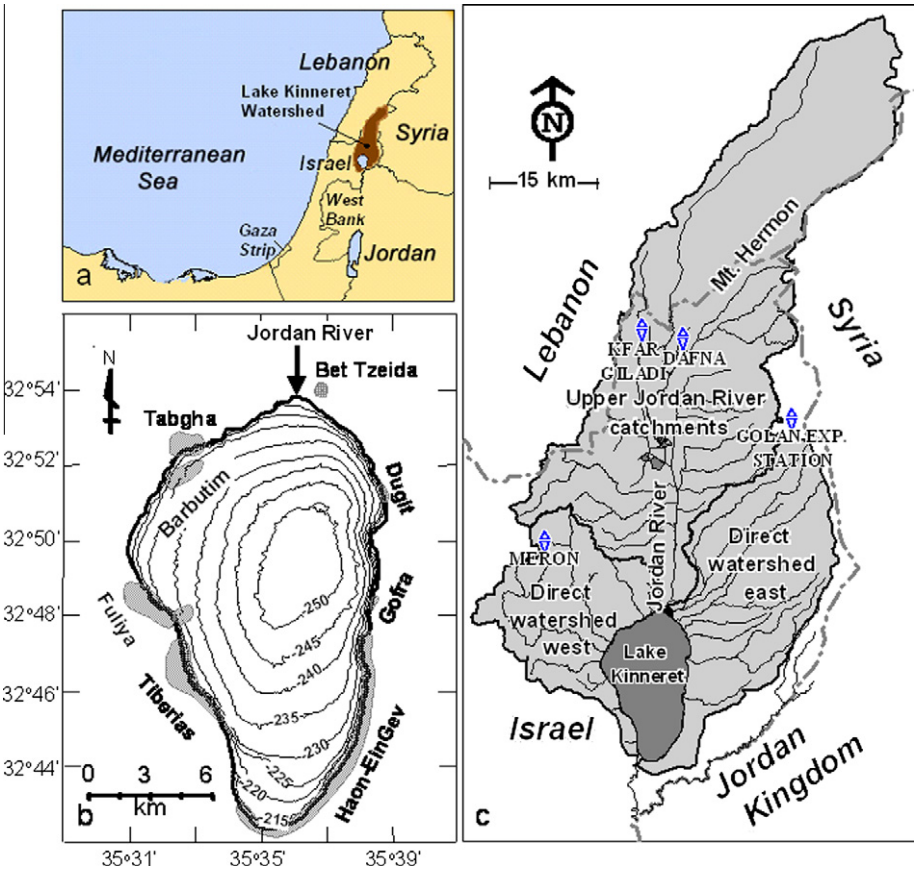

Fig. 1. (a) Orientation map of the east Mediterranean. (b) Lake Kinneret and the regions with saline springs (dark). (c) The Lake Kinneret watershed, including the international borders, the Upper Catchments of the Jordan River, the direct watersheds (east and west), and the four rain gauges displayed in Tables 3.

Hydrological Service, 2009; Mekorot, 1987–2009; Tahal, 1968–1986). An average of ~230 Mm^3 evaporate every year, so that the average annual volume of available water is ~430 Mm^3. Most of this volume is pumped out from the lake every year for consumption, while some water occasionally overflows to the Lower Jordan River towards the Dead Sea.

The annual available water (AW) volumes in Lake Kinneret (AW = sum of all water inflows to the lake, Q_{in}, minus evaporation, E_Y) have exhibited a decreasing trend over the past 60 years. Since 1975, the AW volumes have decreased from 492 Mm^3 to 349 Mm^3 in 2007. Givati and Rosenfeld (2007) showed that the decreasing trend of available water was escorted by decreasing trend in the precipitation on the Golan Heights. Another cause of decreased available water is the increasing consumption in the entire Lake Kinneret watershed (according to the Israeli Water Authority) from 117 Mm^3 in 1975 to 143 Mm^3 in 2007, explaining at least 22% of the total decrease in the AW at this period.

The salinity of Lake Kinerret (190–290 ppm Cl^-) is significantly higher than the salinity of the water from surface streams (20–30 ppm Cl^-) that flow into the lake. It is also higher than the salinity of most groundwater sources in the region. The salinity of the lake is derived mainly from the 40 Mm^3 saline groundwater (average of salinity >1100 ppm Cl^- for the years 1997–2008, *see* Rimmer and Gal, 2003) that emerge through springs along the coasts of the lake. Most of this salinity is from off-shore, unmonitored springs, likely located on the west coast of the lake (Tabgha, Fuliya, Tiberias, Fig. 1b).

3. Model descriptions

This section describes the cascade of various models used in this study (Fig. 2 and Tables 1 and 2). First, the high-resolution climate models and associated data are described. Then the process of bias-correcting the precipitation and calculating evaporation from the meteorological data extracted from the climate models is delineated. These steps are necessary in order to transform the output from the climate model into the appropriate input format for the hydrological models. Then the lake evaporation model (which uses meteorological predictions from the climate model as input), and the water inflows model (which uses precipitation from the climate model as input) are discussed. Finally the structure of the lake salinity model, using the output from the water inflows model and the calculated lake evaporation is clarified. Model verification and future simulations are described in the next sections.

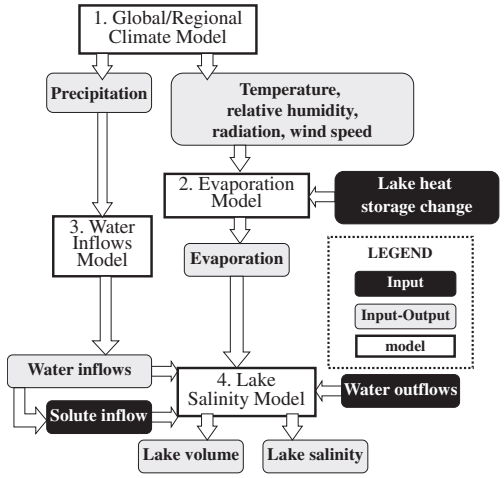

Fig. 2. Schematic description of the proposed cascade of models.

Table 1
Summary of characteristics of four climate models.

Climate model name	ECHAM-RegCM	HADLEY-MM5	ECHAM-MM5	JMA Model
Grid (km)	25	18.6	18.6	20
The model	ICTP RegCM driven by MPI ECHAM5 initial and lateral boundary conditions	MM5 regional model driven by UKMO HadCM3 initial and lateral boundary conditions	MM5 regional model driven by MPI ECHAM5 initial and lateral boundary conditions	Climate-model version of the Japan Meteorological Agency's (JMA) operational numerical weather prediction model
Time period	Transient simulations: 1960–2060			Past (1979–2007) Future (2015–2035)
Output	Daily values for precipitation (P), temperature (T), relative humidity (RH), global radiation (R_s) and wind speed (U)			
Verification	Precipitation: bias correction applied and compare with historical values of rain gauges in UCJR (Fig. 4). Evaporation: compare relevant atmospheric parameters with historic values (Fig. 5)			
Calibration	For precipitation values, bias correction (Déqué, 2007, Fig. 3). For evaporation parameters, no calibration was performed			
Main references	Krichak et al. (2010, 2011), Pal et al. (2007), Roeckner et al. (2006)	Chen and Dudhia (2001), Smiatek et al. (2011), Roeckner et al. (2006)	Chen and Dudhia (2001), Smiatek et al. (2011), Pal et al. (2007)	Mizuta et al. (2006), Kitoh et al. (2008),

Table 2
Summary of three components of the combined model for water availability and salinity in Lake Kinneret (LK).

Characteristic (Equation) [Time interval]	1. LK Evaporation model (LEM) (1), (2) [day]	2. Water inflows model (MRM) (3) [year]	3. LK salinity model (LSM) (4), (5) [year]
Input	Daily values for minimal and maximal temperature (T), relative humidity (RH), global radiation (R_s) and wind speed (U) as extracted from the climate model	Annual precipitation (P) in mm from current and previous year, extracted from the climate model	Annual long term predictions for inflows (Q_{in}) and outflows (Q_{out}) in Mm^3; Annual evaporation values from the lake ($\sum E_D$) in Mm^3; Annual solute inflows (S_{in}) to the lake in ton Cl
Output	Daily evaporation values from the lake (E_D) in Mm^3	Annual long term predictions for incoming water to the lake (Q_{in}) in Mm^3	Long-term predictions of volume (V) in Mm^3, solute mass (S) in ton, and salinity C in ppm Cl^-
Objective	To generate evaporation calculations for use in the water balance and salinity model	To predict annual water inflows to the lake	To use the physical mechanism of complete mixing as a tool to predict long-term changes of chloride concentration in LK
System verification	Compare monthly averaged modeled values with historical values (Fig. 7)	Compare predicted vs. observed values of water inflows (Fig. 6)	Compare predicted vs. observed values of lake volume and salinity from 1964 to 2005 (Fig. 8)
Calibration	No calibration required	Based on regression coefficients	No calibration required
References	Rimmer et al. (2009)	Givati and Rosenfeld (2007)	Rimmer (2003), Rimmer et al. (2006)

3.1. Climate models

Recently, simulations from regional climate models focusing on the Middle East in general and the region of Israel in particular have been generated as part of the GLOWA Jordan River project (http://www.glowa-jordan-river.de). This is a multi-national, interdisciplinary project focusing on sustainable water management in the region. As water resources are directly linked to rainfall, climate simulations are an important driving force for this project. Three climate simulations are currently used each with a different GCM–RCM combination. The first simulation is generated using the Penn State – NCAR MM5 regional model version 3.5 (Chen and Dudhia, 2001; Smiatek et al., 2011) and driven by the ECHAM5-MPI GCM (Roeckner et al., 2006). The second simulation is created using the same regional MM5 model but driven by the UKMO HadCM3 GCM (Collins et al., 2001). The third simulation is based on the ICTP RegCM regional model (Pal et al., 2007) driven by the ECHAM5-MPI GCM (Krichak et al., 2010, 2011).

An additional (forth) high resolution simulation is from a climate-model version of the Japan Meteorological Agency's (JMA) operational numerical weather prediction model with a horizontal grid size of about 20 km (Jin et al., 2010; Kitoh et al., 2008; Mizuta et al., 2006). Currently, this is the only GCM available at this resolution. While the three RCM models used in this study (ECHAM-MM5, Hadley-MM5 and ECHAM-RegCM) are transient climate simulations from 1960 to 2060, the JMA model is a time slice model with a validation period (1979–2007) and a near future simulation (2015–2035). All simulations assume the A1B SRES greenhouse gas emissions scenario where there is a balanced emphasis on all energy sources.

In this study we use precipitation results extracted from the model as well as meteorological parameters necessary for calculating potential evaporation (minimum and maximum temperature, relative humidity, radiation and wind speed). Comparison of the model results with historical data indicated that while most of the parameters used for calculating evaporation were similar, precipitation values from the model for areas of high elevations were underestimated. This is probably due to the complex topography of the region that is still not captured at a 20 km resolution. To fix this discrepancy in the rainfall data, a simple bias correction based on statistical distribution of observed and modeled values was applied. This technique has been previously used on rainfall and temperature data in France (Déqué, 2007) and Israel (Alpert et al., 2008; Samuels et al., 2010). In this bias-correction procedure the daily values from both the observed data and modeled data for the historical period are ordered sequentially. These two time-series are then divided into percentiles and the mean for each percentile is calculated. The bias correction factor (bcf) for each percentile is calculated by subtracting the mean of the modeled data (y) from the mean of the observed data (x) such that $bcf_i = (\bar{x}_i - \bar{y}_i)$. This correction factor is then applied to all the daily values in the modeled time series, including the predicted values, based on the appropriate percentile. By using this method it is assumed that the physical relationships between modeled and real precipitation data will remain constant into the future.

3.2. Lake evaporation model (LEM)

To calculate evaporation from meteorological parameters we used the well known equation of Penman–Monteith (Allen et al., 1998; Valiantzas, 2006) recently adapted for daily evaporation estimates E_D (mm) in Lake Kinneret (Rimmer et al., 2009). The general equation is:

$$E_D = \frac{\Delta}{\Delta+\gamma}(R_n - \Delta G) + \frac{\gamma}{\Delta+\gamma} f(u)(e_{aS} - e_a) \quad (1)$$

where Δ is the slope of the saturation water vapor pressure temperature curve (mbar K^{-1}) calculated using saturated vapor pressure e_{aS} (mbar) and temperature (K), and γ is the psychometric constant (mbar K^{-1}). The first term on the right hand side of Eq. (1) is the 'radiation component' including net radiation R_n on the lake surface (W m^{-2}) and the heat storage change ΔG (W m^{-2}) of the water profile. The second term is the 'wind component' including the wind effect on evaporation, represented by $f(u)$, and the saturated and dry vapor pressure of the air respectively ($e_{aS} - e_a$). The saturated vapor pressure is related to maximum and minimum air temperature and the actual vapor pressure is calculated using the saturated vapor pressure and relative humidity. The usage of the Penman method for deep lakes, where ΔG is significant, requires an a priori estimation for heat storage change. The value of ΔG applied here is the typical daily averaged ΔG, calculated specifically for Lake Kinneret during the years 1987–2008 (Rimmer et al., 2009). Based on past measurements it is assumed that while the annual heat storage in the lake might change under future climatic and lake volume change, ΔG is significantly less sensitive to these changes. Eq. (1) can then be used to calculate daily evaporation rates using input data including maximum and minimum daily average temperature, wind speed, relative humidity and net radiation. The annual summation of the daily evaporation E_D, multiplied by the daily lake surface area A results in the annual amount of evaporation E_Y in Mm^3:

$$E_Y = \sum A \times E_D \quad (2)$$

3.3. The hydrological model

Spatially distributed hydrological modeling of the entire Lake Kinneret watershed is not simple since the watershed includes four different hydrological units: (1) the Jurassic karst region of Mt. Hermon; (2) the basalt plateau of the Golan Heights; (3) the karst of the eastern Galilee Mountains; and (4) the flat alluvial Hula Valley. Each region has different characteristics of geological exposures, soil types and land cover. In addition, the amount of snow, rainfall, and evaporation on Mt. Hermon, the major contributing water source of Lake Kinneret, was not measured systematically prior to 2006. This is because of inaccessibility to most parts of the mountain, and the difficulties in maintenance of meteorological stations at heights above 2000 m ASL (Gilad and Bonne, 1990). A physically based model that attempts to explain the full hydrological process on a short time scale must take into consideration all these spatially distributed variables in the process of validation. However, because of the lack of information, previous daily hydrological models of Mt. Hermon and the Jordan River (Berger, 2001; Rimmer and Salingar, 2006) were only partly based on the spatially distributed climatic input of the region, and mainly used statistical approximations regarding the precipitation and evaporation to the model. For example Rimmer and Salingar (2006) calculated the precipitation on Mt. Hermon by using an extrapolation of the correlation between elevation and precipitation in the north Golan Height, and Samuels et al. (2010) added the HBV snow routine (Hydrologiska Byråns Vattenbalansavdelning) model after Bergström (Bergström, 1995), in order to distinguish between precipitation in the form of snow and rainfall.

Recently, Givati et al. (2011) improved the precipitation modeling for the Mt. Hermon range by using the high resolution (1.3 km) WRF model. However, For annual long term predictions of water inflows into Lake Kinneret, as required in this case, the above daily interval models are by far more complicated but not necessarily more accurate than a simple multiple regression model (MRM) presented here (see the comparison between models performance for annual flow in Section 4.2). The proposed MRM is similar to the empirical type of model, used by the California Department of Water Resources (CDWR, 2003; Roos, 2004). Although the California Sierra Nevada is gauged better than the Mt. Hermon region, and more data are available, the water supply forecasting procedures is based on simple MRM which relate annual snow and rainfall depths to runoff volumes, similar to the process applied here.

The MRM uses annual precipitation data from current year precipitation, and the contribution of the previous year's precipitation. Rainfall is measured at rain gauges located in the upper part of the basin at the Golan Height. The component of previous year precipitation is required because of the ~2.5 year hydrological memory of the Dan Spring component (Rimmer and Salingar, 2006; Givati and Rosenfeld, 2007). The predicted annual incoming water to Lake Kinneret is therefore modeled with:

$$Q_{in(i)} = a \times P_{GH(i)} + b \times P_{GH(i-1)} + c \tag{3}$$

where $Q_{in}(i)$ is the predicted annual (i) incoming water in the lake (Mm^3); $P_{GH}(i)$ is the annual precipitation (mm) on the selected rain gauge on the Golan Height; $P_{GH}(i-1)$ is the annual precipitation (mm) in previous year ($i-1$); and the constant parameters a, b, and c are determined by a calibration process on measured data from the past.

A similar regression model is currently used as an official tool in the Israeli Hydrological Service (IHS) in order to predict the annual amount of available water in Lake Kinneret in response to precipitation on the basin. This model replaced a previous MRM version (Ben-Zvi, 1974; Shentsis and Ben-Zvi, 1999).

3.4. Lake Salinity Model (LSM)

A significant increase or decrease in the salinity of Lake Kinerret may be caused by a change in one of four variables, either individually or simultaneously: (1) Solute inflows to the lake; (2) Freshwater inflows (salinity less than ~40 ppm Cl) from the UCJR and the direct watershed into Lake Kinneret; (3) Water pumped and released from the lake; and (4) Direct evaporation from the lake.

In the past, several models were used to support decisions regarding the operation of the lake as a water resource. In the late 1970s, Eng. F. Mero developed a model for measuring the impact of certain operational aspects, such as pumping and diverting the saline spring, on the salinity of the lake (Mero and Simon, 1992). Ben-Zvi and Benoualid (1981) connected the solute inflow to the semi-annual water discharge and rainfall. Assouline et al. (1994) suggested a monthly-based model for the same purpose, and Berger (2000) developed a general operational model for the Lake Kinneret system. All these models were based on statistical analysis of monthly inflows and outflows to and from the lake, and monthly solute discharge from the saline spring's system, and therefore were rather complicated to operate.

The Lake Salinity Model (LSM) used in this study is a lake-wide system approach model, proposed by Rimmer (2003) and expanded in Rimmer et al. (2006) and Rimmer (2008). It predicts the long term salinity variations of a lake, based on the main components of the annual water and solute balance. However, unlike previous statistical models, it proposes that the salinization process can be described by a simple physically based complete mixing mechanism and therefore can be solved analytically. The solution allows us to easily examine the influence of each component of the solute balance on the expected salinity changes. The model includes both a deterministic component, which results in the "exact prediction" under certain input conditions, and a stochastic component, which shows the possible range of the prediction.

The objective of the LSM in this cascade of models is to predict long-term changes of chloride concentration in Lake Kinneret, based on the input from the hydrological (MRM) and meteorological (LEM) models. The theoretical development of the complete mixing model consists of a simple differential equation for the mass of an inert solute in the lake S (kg), as was described in detail by (Rimmer, 2003):

$$\frac{dS(t)}{dt} + q(t)S(t) = S_{in}(t) \quad \text{Subject to the initial condition } S|_{t=0} = S_0 \tag{4}$$

In this equation the solute mass in the lake $S = C_{lake}V$, is represented by multiplying the average solute concentration in the lake C_{lake} (ppm) by the lake volume V (Mm^3); t is a time unit (year); $S_{in}(t) = Q_{in}(t)\bar{C}_{in}(t)$ is the solute inflow (kg $year^{-1}$), calculated by multiplying the inflow discharge Q_{in} (Mm^3 $year^{-1}$) (including direct rainfall), and the averaged solute concentration of the incoming solute flux $\bar{C}_{in}$ (ppm). It is an integrated value of all solute contributors from the lake exterior, which consists of the lake floor (streams, on and offshore springs) and the water surface (direct rainfall and fallout). The time varying parameter $q(t)$ represents the leaching of the lake ($year^{-1}$), defined as the ratio of annual outflow, Q_{out}, (Mm^3 $year^{-1}$) to lake volume (Mm^3). The leaching q is the reciprocal of annual water residence time (Wetzel, 1983). Finally, S_0 is the initial mass of solute in the lake (kg) at $t = 0$.

Eq. (4) is solved simultaneously with the water balance equation $dV(t)/dt = Q_{in}(t) - Q_{out}(t) - E_Y(t)$, where the predicted annual water inflows and evaporation are needed to calculate the lake volume V. This part of the model is rather trivial annual balance, and was not elaborated here. More details can be found in Rimmer (2003).

The precise expression of solute mass from the linear inhomogeneous equation (4), where $q(t)$ and $S_{in}(t)$ are functions of the time only, can be obtained as a sum of the homogeneous and particular solutions:

$$S(t) = \exp\left(-\int_0^t q(t')dt'\right) \cdot \left[\int_0^t \exp\left(\int_0^{t'} q(t'')dt''\right) S_{in}(t')dt' + S_0\right] \quad (5)$$

Eq. (5) is a fundamental definition of the lake as a natural linear integrator. The solution demonstrate that the changes of solute mass in the lake are the result of integration in time and space of the water, and solute inflows, outflows, lake volume, and evaporation. In the context of the proposed cascade of models, the initial lake volume (V_0, Mm^3) and initial solute mass in the lake (S_0, kg) are determined in advance; the inflows Q_{in} are calculated from Eq. (3) (the incoming water model); the outflows, Q_{out}, are determined from the scenario of water demand chosen; and the lake volume V is calculated from water balance considerations, taking into account the annual evaporation E_Y (Eq. (2)). Finally the solute inflow S_{in} (kg year^{-1}) is approximated as a linear function of the available water ($S_{in} = \alpha \times AW + \beta$), where $AW = Q_{in} - E_Y$ is calculated from both the incoming water model (Q_{in}) and the evaporation model (E_Y). These linear relations were previously shown by Moshe (1978), Ben-Zvi and Benoualid (1981), and Rimmer and Gal (2003). The parameters $\alpha = 44 \pm 9.8$ and $\beta = 84{,}000 \pm 5200$ in the solute inflow equation are statistically significant (P-value < 0.0001), based on calibration of data from the years 1969–2009. The solution (Eq. (5)) assumes that q, S_{in}, and S_0 were deterministic values for a given period. However, in the real world both q and S_{in} may change randomly from one year to another. If a steady lake volume is assumed through the years, the fluctuations of q are mainly a result of various annual outflows, which is directly effected by inflows and evaporation ($Q_{out} = Q_{in} - E_Y$). Similarly, the S_{in} fluctuations are subject to Q_{in} and E_Y. Other deviations from deterministic values are subject to measurement errors, which affect the initial condition S_0. It is therefore proposed that S_{in}, q, and S_0 are better represented by a statistical distribution rather then by a single average value. To that end an uncertainty component was added to each variable of the LSM, in order to estimate not only the expected long-term changes in lake solute mass $S(t)$ and salinity $C_{lake}(t)$, but also the errors associated with this estimation.

Rimmer et al. (2006) show that a similar type of differential equation as Eq. (4) and the solution in Eq. (5) holds for $S^*(t) = S(t) - S_1(t)$, which is the difference between the deterministic solution $S(t)$, and the solution $S_1(t)$ when arbitrary fluctuations in the input are taken into account. Therefore, the complete solution (S_c) with the deterministic (S) and stochastic (S^*) components $S_c = S \pm S^*$ includes the range of possible solute mass fluctuations in time under various changes of S_{in}, q, and S_0.

4. Model verification

4.1. Precipitation and meteorological input from climate models

Precipitation from the climate models were extracted and compared to four rain gauges in the Kinneret basin: (a) the Golan Experimental station, (b) Meron, (c) Kefar Giladi and (d) Dafna. The four time-series were extracted for the specific latitude and longitude using the Grid Analysis and Display System (GrADS) software (Doty and Kinter, 1995). Since the climate models usually underestimated the annual averages as compared with historical data (1979–2009) the statistical bias correction described above was performed. Fig. 3 shows an example of the inverse cumulative distribution functions (CDF, top) and quantile–quantile plots (q–q, bottom) of observed precipitation compared to results of the JMA model for the four chosen gauges. In the CDF, the gray lines are the underestimated modeled results, and the dark lines are the observed rainfall. The bias correction process brings the lower curve up to the level of the upper curve. In the q–q plots (y-axis: modeled and x-axis: observed), the thin crossed lines are values before the bias correction while the dark thick lines are after the bias correction. Table 3 shows the average mean, maximal, minimal and standard deviation of annual precipitation for the Golan Experimental station results from the four models, as well as their deviation in % from the observed precipitation. It should be noted that the comparison of the data and the values used in the hydrological models are annual values, but the statistical bias correction is performed on the daily values. This maintains the seasonality of the time-series as well as the distribution of wet spells and dry spells. The monthly distribution of average precipitation from the climate models is shown (Fig. 4) and compared to the measured monthly precipitation in the Golan Experimental station.

The time series of variables extracted from the climate models for calculating evaporation include minimal and maximal daily

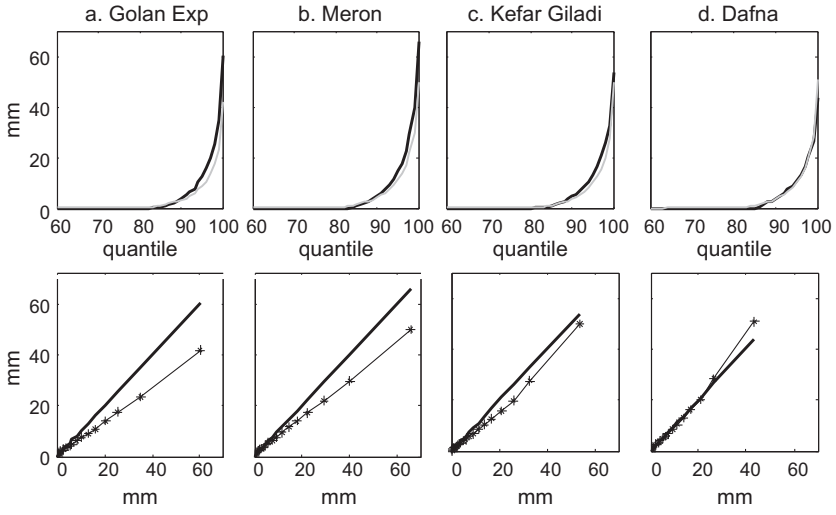

Fig. 3. Inverse CDF (top row) and q–q plots (bottom row) for precipitation based on observed values at four rainfall stations and results from the 20 km GCM model for the years 1979–2007 (28 years): (a) Golan Exp., (b) Meron, (c) Kefar Giadi and (d) Dafna. The inverse CDF shows the percentiles (% along the x axis) of the daily values: observation (dark lines) vs. model output (gray lines) while Q–Q plots show the fit of the observed and modeled data before (crossed) and after (solid) the bias correction.

Table 3
Location and elevation of four selected rain gauges. Mean and standard deviation of average annual values for observed, modeled (using the JMA) and bias-corrected time series are presented.

	Location			Mean			Standard deviation		
	Longitude	Latitude	Elevation (m)	Observed (mm)	Modeled (mm)	After bias correction (mm)	Observed (mm)	Modeled (mm)	After bias correction (mm)
Golan Exp.	35.80	33.13	940	835	567	846	251	174	236
Meron	35.43	32.98	680	879	710	877	270	217	283
Kfar Giladi	35.57	32.24	320	780	652	777	232	199	235
Dafna	35.64	33.23	150	623	650	624	181	197	190

temperature (°C), average daily wind speed (m s^{-1}), daily global radiation (MJ m^{-2}) and average relative humidity (%). Mean annual trends of meteorological parameters can be approximated with an empirical equation of the form $Y = \beta[1 + \alpha \times \sin(\lambda \cdot (JD + \omega))]$ where Y is the parameter being calculated, JD is the day of the year, α and β are constants, ω is the phase shift, and λ is the angular frequency in radians which for characteristics with annual rotations has a set value of $\lambda = 2 \times \pi/365.25$. The typical measured annual trends of the meteorological variables (1996–2009) are illustrated in Fig. 5 in comparison with monthly averaged modeled variables from the climate models. Good agreement between modeled and observed data was found between the maximal daily temperature (Fig. 5b), the global radiation (Fig. 5c) and relative humidity (Fig. 5d). Minimal daily temperature (Fig. 5a) was underestimated by all models, and average wind speed trend (Fig. 5e) was not accurate for all models, and especially overestimated by the EHCAM-RegCM. These inaccuracies are probably the result of the lack of sensitivity of the climate models to the local topography of the lake. Calculated daily evaporation was based on these parameters, and results include their deviations from the measured data.

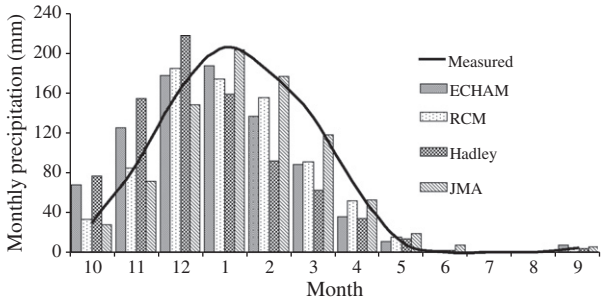

Fig. 4. Monthly averages of precipitation: Columns – calculated from the climate models ECHAM-RegCM, Hadley-MM5, ECHAM-MM5 for the years 1960–2009 and JMA for the years 1979–2009. Line – calculated annual trend in Lake Kinneret based on measurements for the seasons 1996–2008.

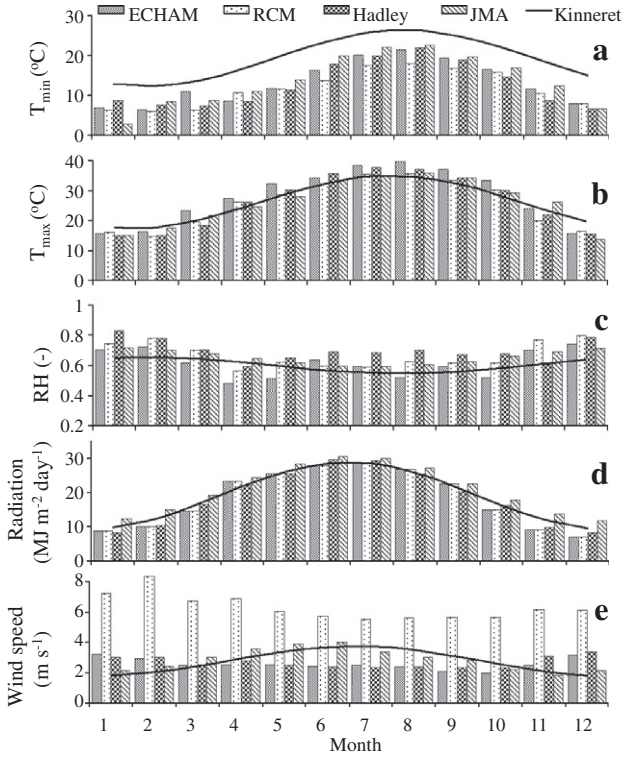

Fig. 5. Monthly averages of the meteorological time series: a. minimal (T_{min}); and maximal (T_{max}) temperature, relative humidity (RH), solar radiation and wind speed. Columns – calculated from the climate models (ECHAM-RegCM, Hadley-MM5, ECHAM-MM5, JMA) for the current situation. Line – calculated annual trend in Lake Kinneret based on measurements for the seasons 1996–2008.

4.2. Incoming water model

In the verification process of incoming water model, the MRM annual prediction for water inflow was tested not only for it's own sensitivity, but also compared to predictions based on a more sophisticated hydrological model (HYMKE, Rimmer and Salingar, 2006).

The MRM uses annual precipitation data from the Golan Experimental Meteorological Station located in the upper part of the basin at the Golan Heights. The rain gauge chosen has the longest measurement history in the area. The constant parameters $a = 1.06 \pm 0.036$, $b = 0.16 \pm 0.035$, and $c = -325 \pm 41$, calibrated for Eq. (3) for the period 1979/1980–2007/2008, are all highly statistically significant (P-value < 0.0002). The correlation between the predicted and observed inflows is $r^2 = 0.97$. This high correlation can be attributed to the fact that at a daily time scale the variations between rain gauge measurements, and the timing of maximum and minimum precipitations are similar for most rain gauges stations in the Golan Heights (Gur et al., 2003), and therefore a single rain gauge has high correlation with other gauges, including those at the Hermon foothills (r^2 ranging between 0.93 and 0.96; Givati, 2006). Due to the topography and geopolitical location of Mt. Hermon, the highest elevation rain gauge with long term available data is Majdal Shams, at 1170 m, located at the southern Hermon range foothills. This rain gauge was operated from 1968/1969 to 1982/1983 and then again since the season of 2000/2001. The annual precipitation ratio of Majdal Shams compared to the Golan Experiment Station (1213 mm $year^{-1}$: 847 mm $year^{-1}$) is 1.42, suggesting strong enhancement of orographic precipitation over the Hermon as compared to the Golan. The correlation between the annual precipitation of Majdal Shams and the Golan experiment station is high ($r^2 = 0.93$) indicating that the selected rain gauge captures the annual variability of rainfall from the Hermon area, the major water contributor to Lake Kinneret. Given this information the high rainfall – stream flow correlation of the water availability model is clarified.

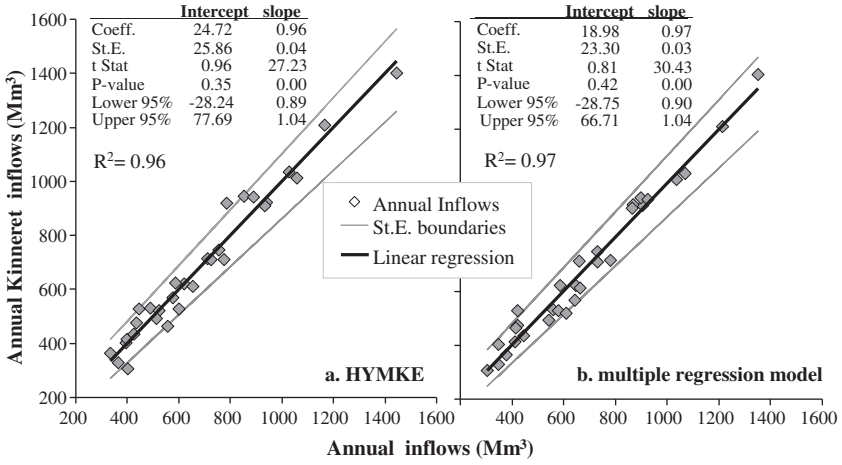

Fig. 6. The relationship between predicted annual inflows (Q_{in}) and measured inflows for the years 1979–2009. (a) Calculated using HYMKE (Rimmer and Salingar, 2006); (b) calculated using the MRM.

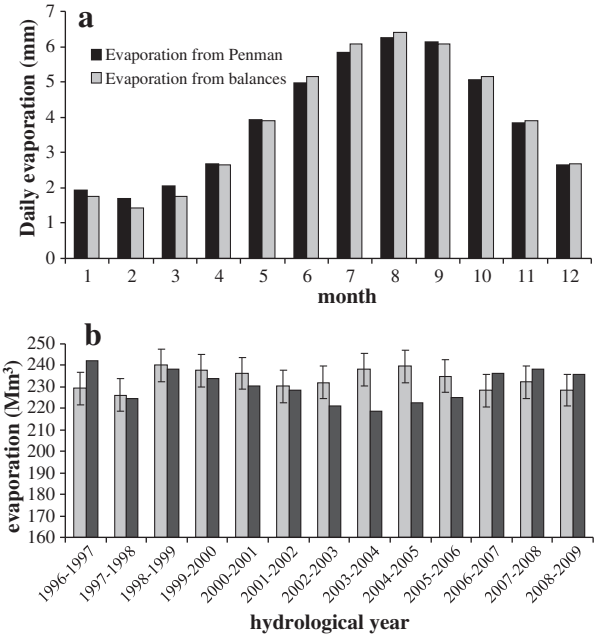

Fig. 7. (a) Monthly calculated average evaporation (mm) from Penman's equation, compared to evaporation from energy balances. (b) Annual evaporation volumes, calculated using Penman's equation, compared to annual evaporation volumes from energy balances for the period 1996–2009. Note the scale of the standard deviation.

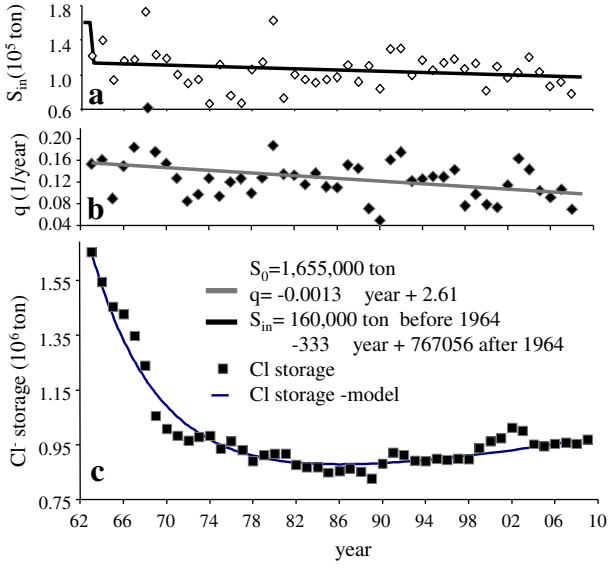

Fig. 8. (a) Step reduction in 1965, followed by a gradual decrease of solute inflow to the lake. (b) Gradual decrease in past water inflows were expressed by a linear decrease of q. (c) The actual salinity of the lake on 1st of October for each year, compared to the model verification as a result of step reduction of S_{in} in 1964 and continuous linear reduction of q.

The other option that was tested to predict annual inflows to Lake Kinneret was to use a well calibrated physically based hydrological model. The Hydrological Model for Karst Environment (HYMKE, Rimmer and Salingar, 2006) is a systems approach, daily precipitation-stream flow model, which was applied simultaneously to the main three tributaries of the Jordan River (Dan, Snir, Hermob). It was verified by comparing the calculated quick and base flow in Mt. Hermon tributaries, with daily measured data over 34 years, which demonstrated good agreement of both the quick flow ($r^2 > 0.6$) and base flow ($r^2 > 0.77$) components. We found that the correlation of cumulative annual flow from HYMKE and measured annual inflow was $r^2 = 0.96$, slightly lower than the correlation with the MRM predictions.

The skill and statistical characteristics of both models in predicting incoming water using historical data are shown in Fig. 6. The simplicity of the MRM compared to HYMKE for annual predictions dictated the use of the MRM for this study, including not only the 'deterministic' linear regression but also the standard deviation range of the prediction.

4.3. Lake evaporation model

Verification of this model was conducted by comparing the annual and monthly evaporation from Eqs. (1) and (2), with the evaporation from the water-solute-heat balances from 1996 to 2009 (Mekorot, 1987–2009). Evaporation from balances can be considered as the best annual estimate we have for evaporation from the lake. The raw data used for model verification (solar radiation, air temperature, relative humidity and wind speed), are the average daily data from Tabgha meteorological station, while heat storage change (e.g. ΔG in Eq. (1)) was assumed as equal to a daily average value, calculated from 1996 to 2009. More details about

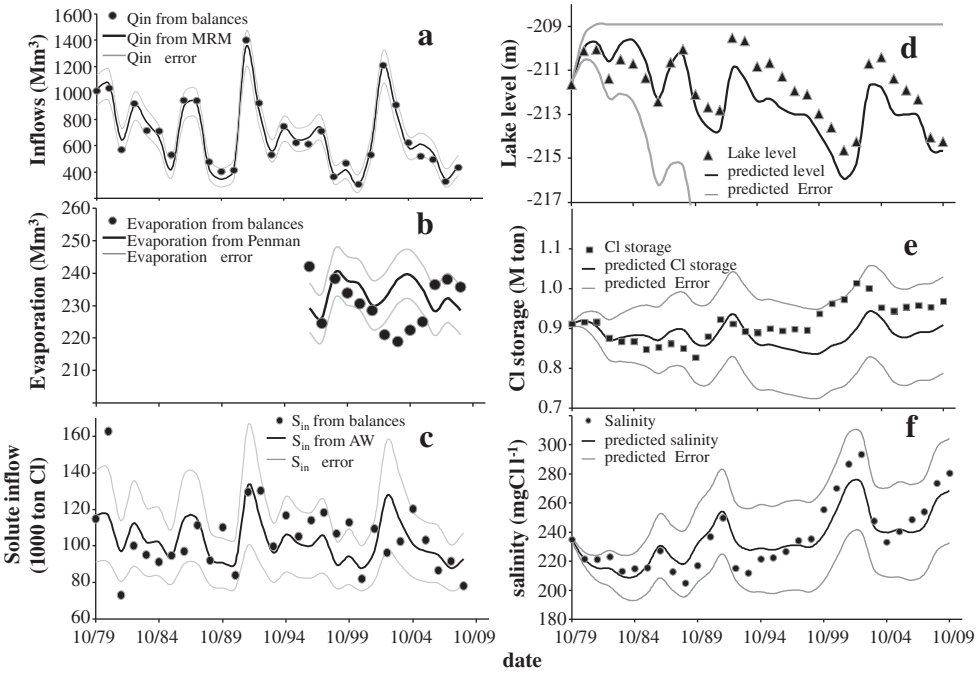

Fig. 9. The process of model verification, conducted with data from 1979 to 2009. (a) water inflows prediction using MRM, compared to inflows from balances; (b) evaporation from the lake, predicted using LEM, compared to evaporation from balances; (c) solute inflows prediction using linear regression with predicted available water (AW), compared to solute inflows from balances; (d) Predicted lake level compared to measured; (e) predicted Cl^- storage compared to measure; (f) predicted Cl^- concentration compared to measured.

this procedure are available in Rimmer et al. (2009). With slight calibration of the 'radiation' and 'wind' components the monthly evaporation rate follows the trend that was calculated from lake balances (Fig. 7a). Average daily evaporation of ~6 mm is typical during August and ~1.5 mm during February. The average annual evaporation predicted by Eq. (1) is 233.35 Mm^3 compared to 230.43 Mm^3 from balances, while the standard deviation of the difference between them is 7.5 Mm^3 (Fig. 7b). In the prediction process of the combined models, this range of error between evaporation from model results and evaporation from balances was taken into account.

4.4. Lake salinity model

The suitability of the LSM was tested and verified by comparing the calculated results of the model with historical lake salinity measurements (Rimmer, 2003). Subsequently, this verification process was expanded to include past solute mass from 1964 to 2009 (see also Rimmer et al., 2006 and Rimmer, 2008). The model helped to identify two dominant processes (Fig. 8): (1) A reduction of the solute mass following a step reduction in S_{in} from $\sim 160 \times 10^6$ to $\sim 105 \times 10^6$ kg $year^{-1}$, as a result of the operation of the Solute Water Carrier during January 1965, and (2) the continuous reduction of inflows (see section *Study Region* above) which resulted in a gradual linear change of q in Eq. (4) from ~0.15 to ~0.10 $year^{-1}$. The cumulative effect of process 1 and 2 is an exponential reduction and a linear increase of solute storage respectively. Both can be seen in the decrease of solute mass in the lake from an average of 1655×10^6 kg in the beginning of the 1960s to 875×10^6 kg during the end of the 1980s (the salinity dropped from ~350 to ~210 ppm Cl), and then a gradual increase back to $\sim 950 \times 10^6$ kg in 2010. During the 1960–1970s the exponential decrease dominated the overall solute storage changes, however since the mid-1980s the exponential decrease has vanished, and the linear increase has become dominant. The understanding of the combination of these processes as well as a verification of past salinity trends indicates that this model can be used successfully for long term salinity predictions, given the expected water and solute inflows, outflows and evaporation.

4.5. Combined models

This section describes a test of performance and a sensitivity analysis of the combined models. The results are illustrated in Fig. 9a–f. Each illustration includes the measured annual values in the past, results of verifications, and standard deviations associated with the verification process. Assuming that the annual precipitation at the Golan Experimental Station is accurate (i.e. without measurement errors) the progress of the model results is as follows: (1) The calibrated MRM (*see* Section 4.2) was used to transfer the annual precipitation into annual inflows, and into the associated standard deviations. According to Fig. 9a inflows prediction is usually good, with average standard deviation of ~92 Mm^3 $year^{-1}$ (~13% of the average inflows). (2) Daily meteorological data were introduced into the LEM, and annual evaporation was calculated for years with available data (1996–2008, Fig. 9b). The difference between the LEM and the balances calculations is attributed mainly to the difference between the two algorithms. While the LEM calculates evaporation based on meteorological and water profile heat measurements only, the balances evaporation significantly rely on the residual of the water balances (Assouline, 1993; Rimmer and Gal, 2003). The standard deviation of evaporation during the 13 years is only ~7.5 Mm^3 $year^{-1}$. The water balance is completed by annual outflows. Since in Lake Kinneret these are subject to operational decisions they were not modeled in the verification, and remained unchanged. (3) With predicted inflows and evaporation, the annual solute inflows and its standard deviations were calculated as a function of available water. As evident from the graph (Fig. 9c) solute inflows are subject to large deviations (standard deviation of S_{in} = ~21,340 ton $year^{-1}$, ~20% of the annual average). (4) Lake level prediction was determined through the predicted volume change (inflows – evapora-

Table 4
Summary of the observed and modeled annual precipitation statistics for the years 1979–2009 using the four climate models. The bias of the modeled precipitation from measured values is given in% in the bottom four rows.

Precipitation 1979–2009 (mm)	Measured	Echam-RegCM	Hadley-MM5	Echam-MM5	JMA model
Average	818.1	780.6	834.8	853.5	846.7
STD	251.6	243.8	304.6	271.7	236.5
Maximal	1495.0	1264.0	1448.4	1554.3	1363.2
Minimal	490.0	252.8	398.5	324.2	299.2
Precipitation bias (%)		−4.59%	2.04%	4.32%	3.49%
STD bias (%)		−3.10%	21.09%	7.99%	−6.00%
Max bias (%)		−15.45%	−3.12%	3.97%	−8.81%
Min bias (%)		−48.40%	−18.67%	−33.84%	−38.93%

tion – outflows) with standard deviation of ∼92.3 $Mm^3\ year^{-1}$ (=0.55 m). Lake volume (and level) is a cumulative result, and therefore the range of cumulative standard deviation around the prediction is large (Fig. 9d). Note however that the maximal difference between predicted and measured lake level in 30 years was only 1.6 m. (5) The predicted Cl^- storage was determined directly from the LSM (Fig. 9e), taking into account the standard deviations of Q_{in} and S_{in} as described above. (6) The predicted Cl^- concentration was determined by dividing the predicted Cl^- storage with predicted lake volume. This same procedure was applied for the upper and lower boundaries of the Cl^- storage (Fig. 9f). The maximal difference between the predictions and measured Cl^- concentration is ∼20 $mgCl^-\ L^{-1}$.

5. Results and discussion

5.1. Water budget: Precipitation, incoming water, evaporation and available water

This chapter demonstrates the use of our cascade of models to predict the long term influence of future climate on incoming water, evaporation, the resulting available water and the salinity of Lake Kinneret. The results are based on climate model predictions for the period 2015–2060 (2015–2035 for JMA). The climate models used are currently the only high resolution models available for the chosen region. For the GCM–RCM combinations, they differ both in the GCM used for initial and lateral boundary conditions as well as in the specific regional model chosen. The JMA model is unique in the sense that it the only global model run at such a high spatial resolution, hence it is not dependant on boundary conditions from other models. It is, however, an uncoupled model, as opposed to the ECHAM and Hadley GCMs which are fully coupled atmospheric-ocean models. These facts as well as some differences in the soil moisture and other schemes can account for the wide range of model results. It has been shown that different climate models exhibit varying performance for varying parameters and in different geographical regions, and hence a combination of models is expected to outperform any single model realization (Doblas-Reyes et al., 2000; Thomson et al., 2006; Weisheimer et al., 2009). In this section we provide results both from the individual model realizations as well as an 'ensemble results' which combines the results from all the models.

Annual precipitation and evaporation were calculated using the data extracted from the climate models, with the same downscaling methods described above for the historical period. Table 4 summaries the downscaled annual precipitation from the climate models, and their bias from the observed precipitation for the years 1979–2009. Fig. 10 shows the predicted annual (a) inflows; (b) evaporation; (c) lake level; (d) solute inflow; and (e) salinity from the four models. It should be noted that in order to keep the predictions with the combined models free of operational decision components, the annual outflows were calculated with an if condition that maintain the lake volume, i.e. (if AW > 0, Q_{out} = AW) thus leaving the lake level steady; but (if AW < 0, Q_{out} = 0) lake level will reduce (Fig. 10c).

Our analysis with the cascade of models focused on the multi annual trends of predicted variables rather then on the absolute predictions, which are subject to large deviations from 1 year to another, and from one model to another. Therefore, in addition to the predicted trends of each variable and for each model, we also show the 'ensemble trend', which stand for the change in time of the average predicted time series. Table 5 presents a trend analysis of predicted annual precipitation ($mm\ year^{-1}$), lake evaporation ($Mm^3\ year^{-1}$), water inflows ($Mm^3\ year^{-1}$) and solute inflows (ton $Cl^-\ year^{-1}$), using the four climate models output for the predicted period, while Fig. 11 presents the 'ensemble results' as well as the 'ensemble trends'. With regard to the single model realizations, the ECHAM-RegCM predicted a significant reduction in precipitation at an average rate of ∼7.5 $mm\ year^{-1}$ (−0.8% annually)

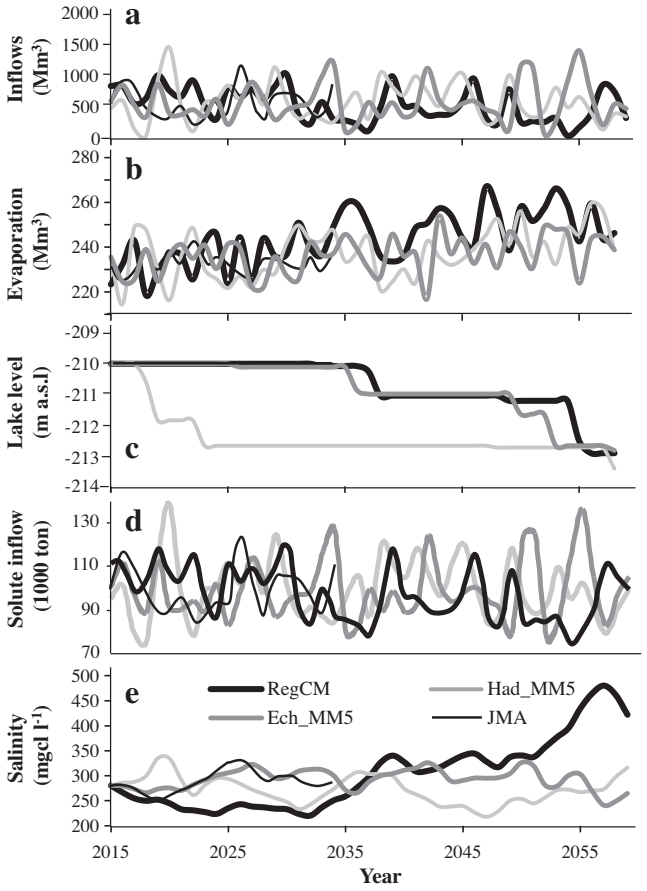

Fig. 10. Combined model results for the years 2015–2060 (JMA only for the period 2015–2035) using output data from climate models. (a) Annual inflows to Lake Kinneret; (b) evaporation from the lake; (c) Lake Kinneret level; (d) solute inflow; (e) Lake Kinneret salinity.

Table 5
Trend analysis of predicted annual precipitation (mm year^{-1}), lake evaporation (Mm^3 year^{-1}), water inflows (Mm^3 year^{-1}) and solute inflows (ton Cl$^-$ year^{-1}), using the four climate models output for the years 2015–2060 (JMA only for the period 2015–2035).

	Echam-RegCM	Hadley-MM5	Echam-MM5	JMA model	Ensemble
Precipitation trend 2015–2060 (mm/year)	−7.472	−1.610	1.631	0.225	−2.229
Evaporation trend 2015–2060 (Mm^3 year^{-1})	0.606	0.374	0.233	−0.051	0.411
Inflows trend 2015–2060 (Mm^3 year^{-1})	−9.054	−1.953	1.943	1.438	−2.599
Solute inflows trend 2015–2060 (ton year^{-1})	−393.820	−71.314	106.433	65.782	−101.218

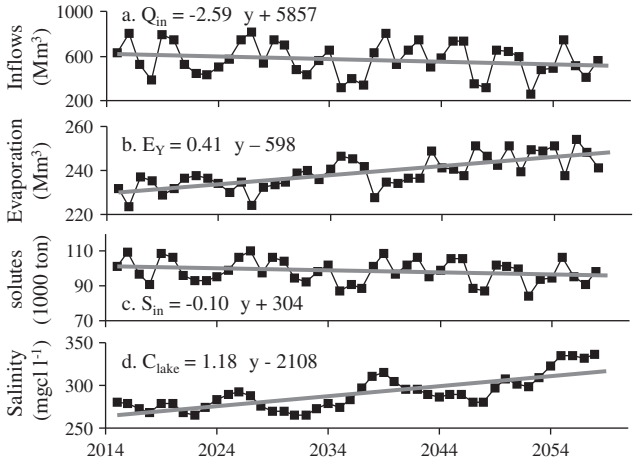

Fig. 11. Ensemble averages and trends: (a) annual inflows to Lake Kinneret; (b) evaporation from the lake; (c) solute inflows to the lake; (d) Lake Kinneret salinity.

while the trends of precipitation predicted by the other models were less pronounced. The combined ensemble trend – a reduction of ~2.2 mm year^{-1} (−0.3% annually) are in agreement with the results of Givati and Rosenfeld (2011) regarding future precipitation in the Lake Kinneret basin. Based on the realizations of the ECHAM-RegCM, Hadley-MM5 and ECHAM-MM5 models with the LEM, the evaporation will increase by 0.6, 0.37 and 0.23 Mm^3 year^{-1} (0.26%, 0.16%, and 0.10%), respectively, while according to the JMA a very small decreasing trend was predicted. The ensemble evaporation prediction was an increase of ~0.41 Mm^3 year^{-1}. The reduced ECHAM-RegCM precipitation, is expected to cause a reduced inflow of ~9 Mm^3 year^{-1} (~1.3% reduction annually), which is significantly larger then the observed decreasing rate of inflows in the past. However, according to the Hadley-MM5 a much smaller reduction (~2 Mm^3 year^{-1}) is expected while the other two models predicted small increase of inflows to the lake. The ensemble prediction for water inflows is a reduction of ~2.6 Mm^3 year^{-1}. The solute inflows trend is mostly impacted by changes in inflows and therefore the ECHAM-RegCM and Hadley-MM5 predicted an annual decrease of 393 and 71 ton Cl$^-$ in the solute mass inflows, respectively, while ECHAM-MM5 and the JMA predict increase of 106 and 65 ton Cl$^-$ respectively. The ensemble prediction was therefore a decrease of 101 ton Cl$^-$ annually.

An important aspect of the general ensemble prediction is the reduced precipitation and increased evaporation. Both changes are shown to cause a cumulative reduction of ~3 Mm^3 year^{-1} in available water. Although it may appear as a significant change, note that the measured reduction of AW from 1975 till present is ~6.5 Mm^3 year^{-1}, more than double that of the predicted reduction.

5.2. Salinity of Lake Kinneret

Previous analysis (Rimmer, 2003) has shown that while evaporative flux and changes in lake level have some effect on the salinity, it is the changes in water and solute inflows that may alter the lake salinity significantly, rendering the other variables less important. In our predictions we used only the available water from the climate and hydrological model to evaluate change in salinity (Fig. 10d). No operational considerations were taken into account, and therefore the result reflects the effect of climate change alone. The predictions of the EHCAM-RegCM for precipitation reduction and increase of evaporation are by far more extreme than the other models, and therefore significant long term changes in lake salinity are expected only with the predictions of this model, while according to the other models, salinity will nearly remain the same until 2060. Combining all salinity predictions together, the expected trend of ensemble salinity is an increase of 1.18 mgCl$^-$ L^{-1} year^{-1} (Fig. 11d).

5.3. Summary

In this study we integrate the results of four global climate models into a water availability and salinity model in order to determine the impact of climate change on water quality and quantity in Lake Kinneret. The results suggest that in addition to changes in precipitation, evaporation from open water sources plays an important role in determining the water budget of the region, and together they have an obvious effect on the future water quality.

This analysis is based on four climate models. These models were shown to skillfully capture past trends, suggesting that they can provide valuable information about the future trends. Of course as more model realizations become available, they can and should be incorporated into this model combination to provide more robust predictions for future change. For now, however, these results can already provide important information for water policy makers and planners.

The salinity of the lake and it's water budget are strongly dependant on operational policy. Such policies include decisions that may have long term effects on lake residence time and salinity. During the past five decades, the lake salinity and residence time were determined mainly by two operational decisions (Rimmer, 2008): (a) the reduction of solute mass flow from the saline springs to the lake by artificial diversion; and (b) the decrease of water inflow to the lake due to an increase in water demand upstream. By examining Fig. 8b and c, and taking into account lake volume of ~4000 Mm^3 it is easy to show that the effect of these two operational policies during the past 50 years caused extended lake residence time from ~7 to ~10 years and reduction in salinity from ~400 to ~220 mgCl$^-$ L^{-1} which are larger then the predicted trends from climatic changes alone.

While this study focuses on a particular region, the methodologies presented are general and can be applied to other water bodies as well.

Acknowledgements

This research is part of the GLOWA – Jordan River Project, funded by the German Ministry of Science and Education (BMBF), in collaboration with the Israeli Ministry of Science and Technology

(MOST). We also want to thank Shimon Krichak and Yosef Breitgard for data from the RegCM and Gerhard Smiatek for data from the MM5 models.

References

Allen, R.G., Pereira, L.S., Raes, D., Smith, M., 1998. Crop evapotranspiration: guidelines for computing crop water requirements. FAO Irrigation and Drainage Paper, 56, Rome, 300 pp.

Alpert, P., Krichak, S.O., Shafir, H., Haim, D., Osetinsky, I., 2008. Climatic trends to extremes: employing regional modeling and statistical interpretation over the E. Mediterranean. Global Planet. Change 63, 163–170.

Assouline, S., 1993. Estimation of lake hydrologic budget terms using the simultaneous solution of water, heat and salt balances and a Kalman filtering approach: application to Lake Kinneret. Water Resour. Res. 29, 3041–3048.

Assouline, S., Shaw, M., Rom, M., 1994. Modeling the solute and water components in Lake Kinneret System. Watershed Unit, Mekorot, Sapir Site, Israel (in Hebrew).

Ben-Zvi, A., 1974. Seasonal forecast for Lake Kinneret. Israel Hydrological Service, Hydro Report 74/3, Jerusalem, Israel (in Hebrew).

Ben-Zvi, A., Benoualid, S., 1981. A model to predict the Lake Kinneret salinization and the solutes storage. Israel Hydrological Service report 1981/5, Jerusalem (in Hebrew).

Berger, D., 2000. Operational Model for the Lake Kinneret System. Watershed Unit, Mekorot Water Supply Co., Sapir Site, Israel (in Hebrew).

Berger, D., 2001. Estimating the natural flow in the upper catchments of the Jordan River, Watershed Unit, Mekorot, Sapir Site, Israel (in Hebrew).

Bergström, S., 1995. Computer models of watershed hydrology. In: Singh, V.P. (Ed.), The HBV Model. Water Resources Publications.

CDWR, 2003. California Department of Water Resources, Water Conditions in California, Sacramento, CA, USA, Bulletin 120.

Chen, F., Dudhia, J., 2001. Coupling an advanced land surface–hydrology model with the Penn State–NCAR MM5 modeling system. Part II: Preliminary model validation. Mon. Weather Rev. 129, 587–604.

Collins, M., Tett, S.F.B., Cooper, C., 2001. The internal climate variability of HadCM3, a version of the Hadley Centre coupled model without flux adjustments. Climate Dynam. 17 (1), 61–81.

Déqué, M., 2007. Frequency of precipitation and temperature extremes over France in an anthropogenic scenario: model results and statistical correction according to observed values. Global Planet. Change 57, 16–26.

Doblas-Reyes, F.J., Deque, M., Piedelievre, J.-P., 2000. Multimodel spread and probabilistic seasonal forecasts in PROVOST. Quart. J. Roy. Meteorol. Soc. 126, 2069–2088.

Doty, B.E., Kinter III, J.L., 1995. Geophysical Data Analysis and Visualization using GrADS. Visualization Techniques in Space and Atmospheric Sciences. NASA, Washington, DC, pp. 209–219.

Gilad, D., Bonne, J.A., 1990. The snowmelt of Mt. Hermon and its contribution to the sources of the Jordan River. J. Hydrol. 114 (1–2), 1.

Givati, A., 2006. Available water model for lake Kinnert. Israeli Hydrological Service, Hydro Report 2006/2/, October, 2006, Jerusalem, Israel.

Givati, A., Rosenfeld, D., 2007. Possible impacts of anthropogenic aerosols on water resources of the Jordan River and the Sea of Galilee. Water Resour. Res. 43. doi:10.1029/2006WR005771.

Givati, A., Rosenfeld, D., 2011. The arctic oscillation, climate change and the effect on Eastern Mediterranean precipitation. J. Climate, submitted for publication.

Givati, A., Rosenfeld, D., Lynn, B., Lui, Y., Rimmer, A., 2011. Using the high resolution WRF model for calculating stream flow in the Jordan River. J. Appl. Meteorol. Climatol., in press.

Gur, D., Bar-Matthews, M., Sass, E., 2003. Hydrochemistry of the main Jordan River sources: Dan, Banias, and Kezinim springs, north Hula Valley, Israel. Isr. J. Earth Sci. 52, 155–178.

IPCC, 2007. Climate change 2007. In: Parry, Martin L., Canziani, Osvaldo F., Palutikof, Jean P., van der Linden, Paul J., Hanson, Clair E. (Eds.), Impacts, Adaptation, and Vulnerability. Contribution of Working Group II to the Third Assessment Report of the Intergovernmental Panel on Climate Change. Cambridge University Press, Cambridge, United Kingdom, p. 1000.

Israel Hydrological Service, 2009. Development and the State of Water Resources Until Autumn of 2009. Israel Hydrological Service, Jerusalem.

Jin, F., Kitoh, A., Alpert, P., 2010. Water cycle changes over the Mediterranean: a comparison study of a super-high-resolution global model with CMIP3. Philos. Trans. Roy. Soc. A 368, 1–13.

Jin, F., Alpert, P., Kitoh, A., 2011. Climatological relationships among the moisture budget components and rainfall amounts over the Mediterranean based on a super-high resolution climate model. JGR-Atmospheres. 116, D09102. doi:10.1029/2010JD014021.

Kitoh, A., Yatagai, A., Alpert, P., 2008. First super-high-resolution model projection that the ancient Fertile Crescent will disappear in this century. Hydrol. Res. Lett. 2, 1–4.

Krichak, S., Alpert, P., Bassat, K., Kunin, P., 2007. The surface climatology of the eastern Mediterranean region obtained in a three-member ensemble climate change simulation experiment. Adv. Geosci. 12, 67–80.

Krichak, S.O., Alpert, P., Kunin, P., 2010. Numerical simulation of seasonal distribution of precipitation over the eastern Mediterranean with a RCM. Climate Dynam. 34, 47–59.

Krichak, S., Breitgand, J., Samuels, R., Alpert, P., 2011. A double-resolution transient RCM climate change simulation experiment for near-coastal eastern zone of the Eastern Mediterranean region. Theor. Appl. Climatol. 103 (1–2), 167–195.

Kunstmann, H., Suppan, P., Heckl, A., Rimmer, A., 2007. Regional climate change in the Middle East and impact on hydrology in the Upper Jordan catchment. IAHS Publication 313, Quantification and Reduction of Predictive Uncertainty for Sustainable Water Resources Management, pp. 141–149.

Mekorot, 1987–2009. The water-solute-energy balances of Lake Kinneret. Annual Report. Mekorot Watershed Unit, Sapir Site, Israel (in Hebrew).

Mero, F., Simon, E., 1992. The simulation of chloride inflows into Lake Kinneret. J. Hydrol. 138, 345–360.

Mizuta, R. et al., 2006. 20-km-mesh global climate simulations using JMA–GSM model – mean climate states. J. Meteorol. Soc. Jpn. 84, 165–185.

Moshe, B., 1978. Information analysis of the saline springs in the west coast of Lake Kinneret. Israel Hydrological Service Report 1978/7, Jerusalem (in Hebrew).

Pal, J. et al., 2007. Regional climate modeling for the developing world: the ICTP RegCM3 and RegCNET. Bull. Am. Meteorol. Soc. 88, 1395–1409.

Rimmer, A., 2003. The mechanism of Lake Kinneret salinization as a linear reservoir. J. Hydrol. 281 (3), 173–186.

Rimmer, A., 2008. System approach hydrology tools for the Upper Catchment of the Jordan River and Lake Kinneret, Israel. Isr. J. Earth Sci. 56, 1–17.

Rimmer, A., Gal, G., 2003. Estimating the saline springs component in the solute and water balance of Lake Kinneret, Israel. J. Hydrol. 284 (1–4), 228–243.

Rimmer, A., Salingar, Y., 2006. Modelling precipitation-streamflow processes in Karst basin: the case of the Jordan River sources, Israel. J. Hydrol. 331, 524–542.

Rimmer, A., Boger, M., Aota, Y., Kumagai, M., 2006. A lake as a natural integrator of linear processes: application to Lake Kinneret (Israel) and Lake Biwa (Japan). J. Hydrol. 319 (1–4), 163–175.

Rimmer, A., Samuels, R., Lechinsky, Y., 2009. A comprehensive study across methods and time scales to estimate surface fluxes from Lake Kinneret, Israel. J. Hydrol.. doi:10.1016/j.jhydrol.2009.10.007.

Roeckner, E., Brokopf, R., Esch, M., Giorgetta, M., Hagemann, S., Kornblueh, L., Manzini, E., Schlese, U., Schulzweida, U., 2006. Sensitivity of simulated climate to horizontal and vertical resolution in the ECHAM5 atmosphere model. J. Climate 19, 3771–3791.

Roos, M., 2004. California cooperative snow surveys program. In: ICID 2nd Asian Regional Conference, Echuca – Moama, Australia.

Samuels, R., Rimmer, A., Alpert, P., 2009. Effect of extreme rainfall events on the water resources of the Jordan River, Israel. J. Hydrol. 375, 513–523.

Samuels, R., Rimmer, A., Hartman, A., Krichak, S., Alpert, P., 2010. Climate change impacts on Jordan River flow: downscaling application from a regional climate model. J. Hydrometeorol. 11 (4), 860–879.

Shaban, A., 2009. Indicators and aspects of hydrological drought in Lebanon. Water Resour. Manage. 23, 1875–1891.

Shentsis, I., Ben-Zvi, A., 1999. Within – season updating of seasonal forecast of Lake Kinneret inflow. J. Hydrol. Eng., ASCE 4, 381–385.

Smiatek, G., Kunstmann, H., Heckl, A., 2011. High resolution Climate Change Simulations for the Jordan River Area. J. Geophys. Res. doi:10.1029/2010JD015313.

Tahal, 1968–1986. The water-solute-energy balances of Lake Kinneret. Annual Report. Tahal, Tel-Aviv (in Hebrew).

Thomson, M.C. et al., 2006. Malaria early warnings based on seasonal climate forecasts from multi-model ensembles. Nature 439, 576–579.

Valiantzas, J.D., 2006. Simplified versions for the Penman evaporation equation using routine weather data. J. Hydrol. 331, 690–702.

Weisheimer, A. et al., 2009. ENSEMBLES: a new multi-model ensemble for seasonal-to-annual predictions: skill and progress beyond DEMETER in forecasting tropical Pacific SSTs. Geophys. Res. Lett. 36 (21), L21711.

Wetzel, R.G., 1983. Limnology. Saunders College Publishing, Fort-Worth, 767 pp.